JOURNAL OF CATALYSIS **161,** 560–569 (1996)
ARTICLE NO. 0218

Charge Transfer in Metal Catalysts Supported on Doped TiO_2: A Theoretical Approach Based on Metal–Semiconductor Contact Theory

Theophilos Ioannides and Xenophon E. Verykios[1]

Department of Chemical Engineering and Institute of Chemical Engineering and High Temperature Processes, University of Patras, GR-265 00, Patras, Greece

Received March 10, 1995; revised January 29, 1996; accepted February 19, 1996

A theoretical analysis of charge transfer in metal catalysts supported on a doped TiO_2 carrier is presented. The development of the theoretical model is based on the metal–semiconductor contact theory and has been used to calculate the amount of charge transferred to supported metal crystallites, as a function of the electronic structure of the semiconducting support and the metal crystallite size. It is shown that TiO_2, doped with higher valence cations, has unique properties which favor the transport of charge at the interface. The quantity of charge transferred is found to be as high as 0.5 electrons per metal atom for crystallites smaller than 2 nm or negligible for crystallites larger than 10 nm. The effect of charge transfer on the electronic structure of supported metal crystallites is discussed.

INTRODUCTION

The concept of modification of the catalytic properties of supported metals (or oxides), via a mechanism involving electronic interactions at the metal–support interface, originated in early works of Schwab (1) and Solymosi (2). Their methodology was based on the alteration of the electronic structure of semiconducting carriers by altervalent cation doping in order to control the direction and the amount of charge transferred between the metal and the support, as predicted by the metal–semiconductor contact theory. This approach was also followed by others at the time (3).

The Strong Metal-Support Interaction (SMSI) phenomenon is the most widely studied concept of metal–support interactions. Although a geometric model (migration of reduced support species onto the metal surface) has been able to account for the majority of experimental observations (4–7), experimental results obtained by spectroscopic techniques (8–12) or conductivity measurements (13, 14) on M/TiO_2 catalysts have been claimed to provide indications for electron transfer from the TiO_2 support to the metal.

Electron transfer to the metal or, generally, an electronic interaction in systems of the form M/TiO_2 has been proposed by many investigators to account for observed changes in the adsorptive and catalytic properties of the supported metal particles. This model has been used by Solymosi *et al.* (15) to explain the enhanced activity of Rh/TiO_2 catalysts in the hydrogenation of CO and by Mériaudeau *et al.* (16) for the activity pattern of Pt/TiO_2, Ir/TiO_2, and Rh/TiO_2 in the SMSI state. The decrease of the adsorption strength of CO on Pt/TiO_2 (7) and Ni/TiO_2 (17) and of H_2 on Pt/TiO_2 (18) has also been attributed to an electronic interaction.

Electron transfer from the support to the metal has been proposed in the case of Ru catalysts supported on alkaline earth (19) or 19 different kinds of oxides (20). In both cases, the adsorptive and catalytic behavior of Ru was correlated with the electronegativity of the support, which is a measure of its electron donating properties. Electronic interactions were also investigated in the case of Cu supported on several semiconducting oxides (21). Increased activity of Cu in the hydrogenation of CO was observed, when Cu was supported on high work function *p*-type semiconductors, such as ZrO_2 or Cr_2O_3, and it was attributed to electron transfer from Cu to the support.

Metal–TiO_2 junctions have been studied experimentally as potential hydrogen sensors (22). It was found that contacts of Pd or Pt with TiO_2 are of the Schottky type (which results from electron transfer from the semiconductor to the metal) under ambient air, while they become ohmic under high hydrogen concentrations. This was attributed to changes of the work function of the metal in different gas atmospheres.

The effect of altervalent cation doping of TiO_2 on the adsorptive and catalytic properties of supported metal catalysts has been the subject of extensive research work in this laboratory. Doping of TiO_2, which takes place via dissolution of heterovalent cations in the TiO_2 matrix, can be described by the valence induction law initially developed by Verwey *et al.* (23). It has been found that the chemisorption capacity and activity of Pt is significantly suppressed when it is supported on TiO_2 doped with higher-valence cations, while it is not affected when supported on TiO_2 doped with

[1] To whom correspondence should be addressed.

0021-9517/96 $18.00

lower-valence cations (24–27). The reverse behavior was observed for Rh, which, when supported on higher-valence doped TiO_2, exhibits enhanced catalytic activity (27–29). Similar results were also obtained by Solymosi *et al.* (30) for Rh catalysts in the CO/H_2 reaction. The strength of the adsorption bond of CO on Pt dispersed on higher-valence doped TiO_2 is weakened, as deduced from IR experiments (25). A similar result was also obtained for Rh catalysts employing TPD (31) and FTIR spectroscopy (32). Doped catalysts have also been tested in hydrogenation reactions of aromatics, where enhanced activity was found for Rh, Ru, and Pd, but reduced for Pt (33, 34). Electrical conductivity measurements of the doped TiO_2 supports have shown that doping with higher-valence cations leads to an increase of the *n*-character of TiO_2, while no significant effect is observed for lower-valence cation doping (35). The correlation found between the conductivity characteristics of the support and the catalytic properties of the supported metal particles was considered as further evidence for the existence of a metal–support interaction of the electronic type, based on the metal–semiconductor contact theory (24–34).

It is apparent that a metal–support interaction of the electronic type has often been proposed to account for results obtained either in a spectroscopic investigation or in characterization of the adsorptive and catalytic behavior of supported metal catalysts. The majority of the research work has focused on Group VIII metals supported on TiO_2 (doped or not). The metal–semiconductor contact theory offers an attractive approach for describing the electron transfer process quantitatively. Such calculations have been performed by Baddour and Deibert for a Ni/Ge contact (3), while an analysis for Pt supported on doped TiO_2 can be found in Refs. (24) and (26). An estimate of the amount of charge transfer together with a brief analysis is also given in Ref. (36). However, these studies have not clearly shown how the electron transfer process depends on the metal crystallite morphology and size and on the properties of the semiconducting carrier.

In the present work, a model based on the metal–semiconductor contact theory has been employed for the calculation of the number of electrons transferred to the metal crystallite, as a function of the electronic structure of the support and the metal crystallite size. Calculations were carried out for a typical Group VIII metal in contact with a doped TiO_2 support, but they bear general implications.

THEORETICAL MODEL

(a) Metal–Semiconductor Contact Theory

The condition of thermodynamic equilibrium in a metal–semiconductor contact states that the electrochemical potential should be uniform throughout the system. If, before contact, the metal and the semiconductor have different electrochemical potential, then upon contact, charge will flow to the material with the smaller potential, until the potentials are equalized. When the two materials have no net charge, it is

$$\begin{aligned} \tilde{\mu}_e^M &= -\Phi_M \\ \tilde{\mu}_e^{SC} &= -\Phi_{SC}. \end{aligned} \qquad [1]$$

(A list of symbols is given in Appendix 2.) If $\Phi_M > \Phi_{SC}$, the electron flux will be toward the metal. At equilibrium, the common electrochemical potential will be

$$\tilde{\mu}_e^{eq} = -\Phi_M - e\Psi_M = -\Phi_{SC} - e\Psi_{SC} \qquad [2]$$

and

$$\Delta\Phi_M^{SC} = -e\Delta\Psi_M^{SC}; \qquad [3]$$

that is, a contact potential difference equal to the work function difference has developed. Ψ_M and Ψ_{SC} refer to the outer potential of the metal and the semiconductor, respectively. The contact of a metal with an *n*-type semiconductor, in the situation in which $\Phi_M > \Phi_{SC}$, is shown schematically in Fig. 1. Electrons which are transferred to

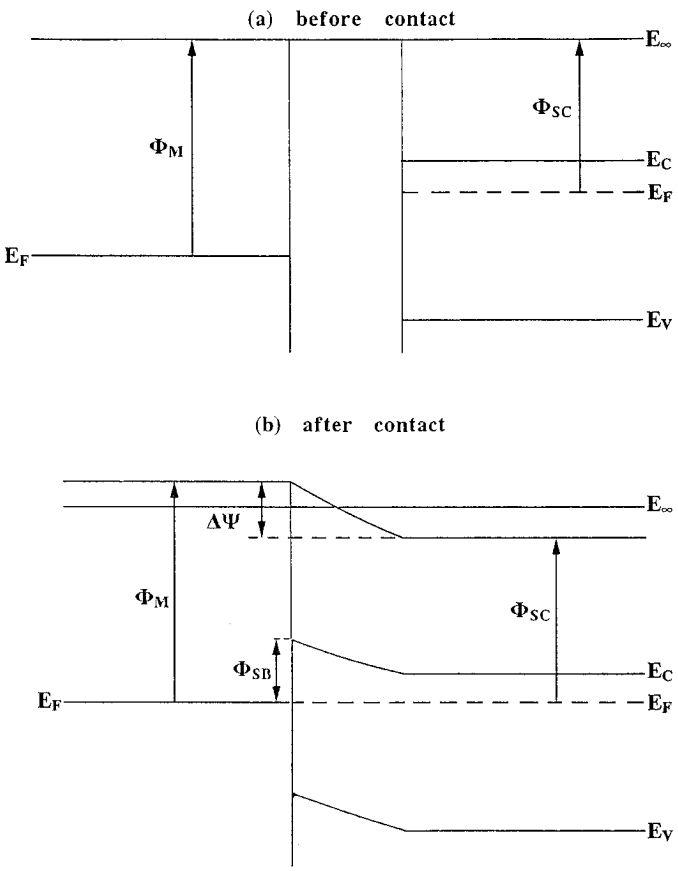

FIG. 1. Contact of a metal with work function Φ_M, with an *n*-type semiconductor with work function, Φ_{SC}; $\Phi_M > \Phi_{SC}$: (a) before and (b) after contact.

the metal are contained at the interface atoms, while the region in the semiconductor which is depleted of electrons is characterized by bending of the valence and conduction bands (37–41). The Schottky barrier, Φ_{SB}, at the interface is

$$\Phi_{SB} = (\Phi_M - \Phi_{SC})/e. \quad [4]$$

Covalent semiconductors, such as Si, GaAs, have a large density of surface states in the band gap causing pinning of the barrier (37). On the other hand, ionic semiconductors, such as ZnO, have low density of surface states in the band gap and the barrier height does indeed depend on the work function difference between the metal and the semiconductor. It has been shown that for strongly ionic semiconductors the barrier height will indeed be equal or proportional to the work function difference (37, 38), as Eq. [4] indicates. Because TiO_2 is an ionic semiconductor, it is logical to assume that the ideal Schottky theory can be used to describe a metal–TiO_2 contact; experimental evidence also supports this hypothesis. The barrier height in contacts of TiO_2 with metals, such as Pd, Pt, or Au under air, was experimentally found to be equal to the work function difference (22), as Eq. [4] predicts.

(b) Poisson Equations: Infinite Interface

A mathematical model of metal–semiconductor contacts is employed to estimate the quantity of charge transferred through the interface, based on parameter values which pertain to the M/TiO_2 system which is of interest in the present study. The direction of electron flux in a metal–semiconductor contact depends upon the relative values of the work function of the two materials. The work function of the semiconductor is a function of the kind (valence) and concentration of the dopant and of temperature. Doping of the TiO_2 carrier with cations of higher valence (e.g., W^{6+}) enhances significantly its electrical conductivity (35), which can be attributed to the creation of donor levels near the lower edge of the conduction band. As a consequence, the Fermi level of TiO_2 is shifted upward, closer to the conduction band, and the work function decreases. Therefore, the Schottky barrier will be higher in the case of TiO_2 doped with higher-valence cations.

The process of electron transfer to the metal leads to the creation of a positively charged region in the semiconductor, for which the Poisson equation applies:

$$\nabla^2 V = -\frac{\varrho(x, y, z)}{\varepsilon_S}, \quad [5]$$

where $\varrho(x, y, z)$ is the charge density and ε_S is the permittivity of the semiconductor; $\varepsilon_S = \varepsilon\varepsilon_o$, where ε is the static dielectric constant of the semiconductor and ε_o is the vacuum permittivity. If it is assumed that the concentration of positive holes in the semiconductor is negligible (this is true in the case of an *n*-type semiconductor doped with a donor impurity), then ϱ can be expressed (39) as

$$\frac{\varrho}{e} = N_d - \frac{N_d}{1 + \frac{1}{2}\exp((-eV - E_d)/kT)} - n_\infty \exp\left(\frac{eV + E_F}{kT}\right), \quad [6]$$

where N_d represents the donor concentration, n_∞ is the electron concentration in the bulk of the semiconductor, and E_d is the donor energy level. Details of the derivation of Eq. [6] are given in Appendix 1. At small distances from the interface, where V is appreciable, the second and third right-hand-side terms are negligible, compared to the first term. The closer the donor level, E_d, is to the conduction band, the larger the distance that the first right-hand-side term will predominate. Neglecting the second and the third terms, Eq. [6] becomes

$$\frac{\varrho}{e} = N_d. \quad [7]$$

For an infinite metal–semiconductor interface the electrostatic potential, V, in the depletion region depends only on the distance, x, from the interface. Using Eq. [7], the Poisson equation becomes

$$\frac{d^2V}{dx^2} = -\frac{eN_d}{\varepsilon_S}, \quad 0 \le x \le W$$

$$\frac{d^2V}{dx^2} = 0, \quad x \ge W \quad [8]$$

with boundary conditions, $V(x=0) = V_0 = (\Phi_M - \Phi_{SC})/e$ and $V(x=W) = 0$, where W is the length of the depletion region. The electric field, F ($F = dV/dx$), at the interface is obtained via integration of Eq. [8]:

$$F = \frac{eN_d W}{\varepsilon_S} \quad [9]$$

while the depletion length, W, is

$$W = \left(\frac{2\varepsilon_S |V_0|}{eN_d}\right)^{1/2} \quad [10]$$

and the electric charge per unit of interface area, Q, which is transferred to the metal, is

$$Q = eN_d W = (2\varepsilon_S e N_d |V_0|)^{1/2}. \quad [11]$$

At larger distances from the interface, the assumptions leading to Eq. [7] are not applicable. If Eq. [6] is used as the expression for ϱ, the Poisson equation becomes

$$\frac{d^2V}{dx^2} = -\frac{e}{\varepsilon_S}\left[N_d - \frac{N_d}{1 + \frac{1}{2}\exp((-eV - E_d)/kT)} - n_\infty \exp\left(\frac{eV + E_F}{kT}\right)\right] \quad [12]$$

with boundary conditions, $V(x=0)=V_0$ and $V(x=\infty)=0$. This equation can be solved numerically.

(c) Finite Interface

The analysis presented above refers to an infinite interface. A real interface can be considered as infinite, when its characteristic size is significantly larger than the depletion length of the semiconductor, i.e., generally much larger than 10–50 nm. Because the metal crystallites in supported catalysts are very small, in the range of 1–10 nm, the aforementioned one-dimensional model cannot be applied with significant accuracy, so that the Poisson equation in the three-dimensional form (Eq. [5]) has to be employed instead. Metal crystallites are usually represented as semispherical particles resting on top of the support surface. Obtaining the solution in this case is quite a formidable task and in order to overcome this difficulty, a physical model with spherical symmetry was employed and is presented in Fig. 2. The model consists of a spherical metal particle of radius, r_M, embedded in the semiconductor bulk. Although this model has no practical significance, its solution can be obtained in a straightforward manner because of the spherical symmetry. By applying the Gauss theorem (42) and using Eq. [7] to represent the charge density in the depletion region, the following relationship for the electric field can be obtained:

$$F = \frac{eN_d}{3\varepsilon_S r^2}(W^3 - r^3), \quad r_M \le r \le W$$
$$F = 0, \qquad r \ge W. \qquad [13]$$

The potential, V, can be calculated upon integration of Eq. [13] ($F = dV/dr$),

$$V = \frac{eN_d}{\varepsilon_S}\left(\frac{W^2}{2} - \frac{r^2}{6} - \frac{W^3}{3r}\right) \quad r_M \le r \le W$$
$$V = 0, \qquad r \ge W, \qquad [14]$$

and the contact potential is

$$V_0 = \frac{eN_d}{\varepsilon_S}\left(\frac{W^2}{2} - \frac{r_M^2}{6} - \frac{W^3}{3r_M}\right). \qquad [15]$$

Equation [15] can be used for the determination of W as a function of V_0, N_d, and r_M. The dependence of the depletion length, W, on the radius of the metal particle, r_M, has to be noted. All other parameters being the same, W decreases with decreasing metal particle size. This does not happen in the case of an infinite interface, where W does not depend on the thickness of the metal layer. The number of electrons transferred to the interface, n_e, is the product of the charge density, N_d, and the volume of the depletion region, $4\pi(W^3 - r_M^3)/3$:

$$n_e = \frac{4\pi N_d}{3}(W^3 - r_M^3). \qquad [16]$$

At this point the assumption is made that this analysis pertains also to the case of a spherical metal particle, half of which is embedded in a semiconductor surface. This physical model which is employed to simulate a metal crystallite supported on the TiO_2 surface is presented in the lower part of Fig. 2. This configuration is obtained by removing the upper half of the semiconductor, thereby exposing half of the spherical metal particle to the gas phase. In this way the spherical symmetry is maintained and to a first approximation the number of electrons transferred will simply be half the amount predicted by Eq. [16].

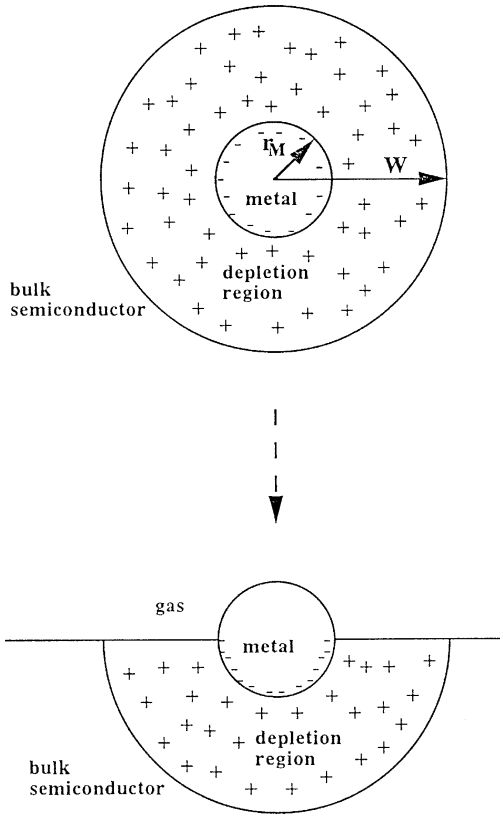

FIG. 2. Physical model used to simulate the contact of a metal crystallite with a semiconducting support.

RESULTS

(a) Infinite Interface

It is obvious from Eq. [11] that the charge transferred per unit interfacial area, Q, is proportional to the square root of V_0, N_d, and ε_S. The absolute value of the contact potential difference, $V_0 = (\Phi_M - \Phi_{SC})/e$, will, typically, be in the range 0–2 V, since a typical value for the metal work function is 4.5–6.0 eV, while the work function of donor-doped TiO_2 is 4.0–4.5 eV (see Appendix 1 and Table 1). The donor concentration, N_d, is proportional to the dopant

TABLE 1

Charge per Unit Area, Q, Transferred to the Metal, as a Function of N_d and Φ_M ($E_d = 0.2$ eV, $T = 500$ K, $\chi_{SC} = 4.0$ eV)

N_d (cm^{-3})	Φ_M (eV)	Φ_{SC} (eV)	V_0 (V)	W (nm)	Q (e/nm^2)
5×10^{19}	5.0	4.117	0.883	15.9	0.795
1×10^{19}	5.0	4.154	0.846	34.8	0.348
1×10^{18}	5.0	4.212	0.788	106.2	0.106
1×10^{17}	5.0	4.282	0.718	320.5	0.032
2×10^{20}	6.0	4.090	1.910	11.7	2.340
5×10^{19}	6.0	4.117	1.883	23.2	1.160
1×10^{18}	6.0	4.212	1.788	160.0	0.160

concentration and is in the order of 10^{20} cm^{-3} for dopant concentration in the range 0.1–0.5 at%, assuming that the dopant is of valence +6. The permittivity, ε_S, $\varepsilon_S = \varepsilon\varepsilon_o$, of TiO_2 is very large. TiO_2, especially in its rutile form, has an unusually high static dielectric constant, ε. An average value of 130 has been used by Akubuiro and Verykios (24), while values in the range 110–117 are also given elsewhere (43). By comparison, the dielectric constant of other oxides is, generally, in the range 5–15. Therefore, only due to the difference in dielectric constant, the charge transferred in the case of TiO_2 will be three to four times larger than for other typical semiconducting oxides. The electric field at the interface, on the other hand, will be weaker, since it is inversely proportional to the square root of the semiconductor permittivity (Eq. [9]).

Some preliminary calculations were performed in order to identify whether the simplified form of the charge density equation, Eg. [7], is adequate for the purposes of this study. Eq. [12] was solved numerically employing a fourth-order Runge–Kutta method. The model parameters used correspond to donor-doped TiO_2 (doped with higher valence cations) in contact with a metal with work function of 5 eV. The donor energy level, E_d, was assumed to be 0.2 eV (referenced to the lower edge of the conduction band) and the donor concentration, N_d, 5×10^{19} cm^{-3}. The charge density, ϱ, and potential, V, as computed from Eqs. [8] and [12] are shown as a function of the distance x from the interface in Figs. 3a and 3b, respectively. While Eq. [12] represents in a more realistic way the charge density distribution in the semiconductor, it can be seen from Fig. 3a that the charge density is indeed equal to N_d close to the interface, as Eq. [7] assumes. However, what is of interest in this study is the number of electrons transferred. From this aspect, the two models are equivalent, since approximately the same number of electrons transferred is found in both cases. For example, Eq. [8] predicts a charge transfer of 0.79 e/nm^2, while Eq. [12] predicts 0.74 e/nm^2, using the parameters of Fig. 3. Similar agreement is observed for other parameter values, such as $N_d = 10^{18}$ cm^{-3}, where the amount of charge transferred is estimated to be 0.106 and 0.102 e/nm^2, respectively. For this reason, all subsequent calculations were made using Eq. [7] for the charge density.

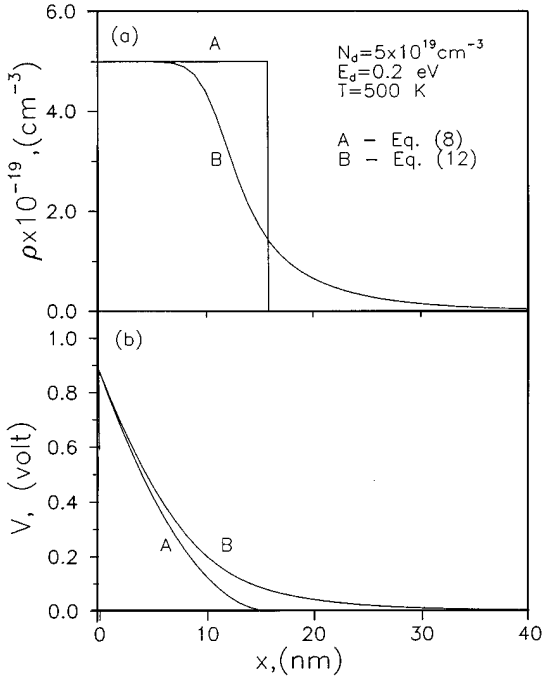

FIG. 3. Charge density, ρ, and potential, V, in the semiconductor depletion region as computed from Eqs. [8] and [12].

The quantity of charge transferred per unit interfacial area, or charge transfer flux, Q, for different values of N_d and Φ_M is given in Table 1. Values of other parameters employed are $E_d = 0.2$ eV, $T = 500$ K, and the semiconductor electron affinity 4.0 eV, corresponding to the value of TiO_2. The work function of doped TiO_2, Φ_{SC}, was calculated according to the method described in Appendix 1. The charge transfer flux, Q, is in the range of 0.1–2.5 e/nm^2. The maximum flux predicted is less than 2.5 e/nm^2, using meaningful values for the model parameters. The depletion length, W, is in the range 10–300 nm, while for a rather heavily doped semiconductor, W will generally be in the range 10–50 nm. The atom surface density for a Group VIII metal is approximately 13 nm^{-2}; therefore the maximum charge transferred per interface metal atom is 0.2 e. Calculations by Baddour and Deibert (3) for a Ni/Ge contact show a maximum charge transfer of about 0.1 e/nm^2 or 0.008 e/atom, while Ponec (36) suggests a value of 0.003 e/atom for $N_d = 10^{18}$ cm^{-3}, $V_0 = 2$ V, and $\varepsilon = 10$. These results agree well with results in this work for low levels of doping. However, as stated earlier, the high dielectric constant of TiO_2 ($\varepsilon = 130$) and the addition of dopant lead to larger amounts of charge transferred.

Another important parameter is the ratio of the number of transferred electrons to the *total* number of metal atoms, e/M. This parameter is used in a phenomenological manner in the context of this work and it is not implied that

TABLE 2

Ratio *e*/*M* of Electrons Transferred over the Total Number of Metal Atoms, for an Infinite Metal Layer in Contact with Doped TiO_2 ($E_d = 0.2$ eV, $T = 500$ K, $\chi_{SC} = 4.0$ eV)

N_d (cm^{-3})	Φ_M (eV)	Layer thickness (Å)	*e*/*M*
5×10^{19}	5.0	2	0.055
5×10^{19}	5.0	4	0.027
5×10^{19}	5.0	6	0.018
5×10^{19}	5.0	10	0.011
2×10^{20}	6.0	2	0.161
2×10^{20}	6.0	4	0.081
2×10^{20}	6.0	6	0.054
2×10^{20}	6.0	10	0.032

each metal atom bears this charge. The transferred charge is contained at the metal–semiconductor interface. Considering an infinite metal layer, the ratio *e*/*M* will depend on the layer thickness. Results of *e*/*M* as a function of layer thickness are presented in Table 2. The maximum value of *e*/*M* predicted is about 0.10–0.15 *e*/atom for a layer one or two metal atoms thick. Kao *et al.* (9) estimated a value of 0.1 *e*/Ni for a Ni monolayer on TiO_2 (100), although they did not observe any band bending of TiO_2 and they proposed that the charge is transferred from surface Ti^{3+} species. Sadeghi and Henrich (10) estimated a charge transfer of about 10^{15} *e*/cm^2 to a Rh monolayer from surface Ti^{3+} species of reduced TiO_2. This charge corresponds to a ratio *e*/Rh of 0.69 for a Rh layer 0.2 nm thick. It is noteworthy that calculations from this work, based on the metal-semiconductor contact theory, predict, for the case of TiO_2, a charge transfer of the same order of magnitude as the one observed for model metal catalysts on TiO_2 crystals.

(b) Finite Interface

The finite interface model was used to calculate the number of transferred electrons, n_e, as well as the ratio *e*/*M*, as a function of the diameter of the metal crystallite, *d*. The parameters employed correspond to a metal with work function of 5.0 or 6.0 eV (the corresponding contact potential differences, V_0, being 0.9 and 1.9 V, respectively), in contact with TiO_2 doped with a donor impurity (W^{6+}, for example) with donor concentration, N_d, equal to 2×10^{20} cm^{-3}. The results obtained are shown in Fig. 4, in which the number of transferred electrons, n_e, and the ratio *e*/*M* are plotted as a function of metal crystallite size, *d*. The number of transferred electrons, n_e, ranges from about 8000 electrons for a 40-nm metal particle to approximately 60 electrons for a 1.5-nm particle. It can be seen that the ratio of the number of transferred electrons to the number of total metal atoms in the crystallite, *e*/*M*, is less than 0.01 for crystallites larger than 10 nm, but can be as high as 0.5 for 1.5 nm crystallites.

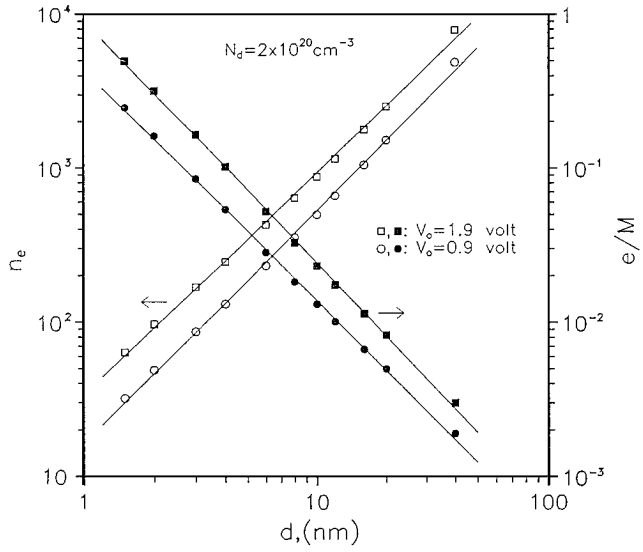

FIG. 4. Number of transferred electrons, n_e, and the resulting ratio, *e*/*M*, as a function of the metal crystallite diameter, *d*.

The latter value is of the same order of magnitude as the one found for a metal layer of one or two atoms thick and defines an upper limit for the ratio *e*/*M*, using meaningful values for the model parameters. The number of transferred electrons, n_e, and the ratio, *e*/*M*, are almost directly proportional to the contact potential, V_0. The ratio *e*/*M* is approximately proportional to $d^{-1.5}$, or alternatively to $D^{1.5}$, where *D* is the metal dispersion. The number of transferred electrons was also found to be a weak increasing function of N_d. At low donor concentrations the depletion length increases and a much larger volume of the semiconductor is depleted of electrons.

The presence of a fairly strong dipole at the metal–support interface leads also to the creation of strong electrostatic fields in this region. Predictions of the magnitude of the electrostatic field can be obtained via Eqs. [9] or [13] and are presented in Table 3. Typical estimated values are in the range 10^6–10^7 V/cm or 0.1–1 V/nm. The finite interface model predicts that the electric field will be dependent on the crystallite diameter, being more intense for small metal

TABLE 3

Estimated Electric Field at the Metal-TiO_2 Interface ($E_d = 0.2$ eV, $T = 500$ K, $\chi_{SC} = 4.0$ eV)

N_d (cm^{-3})	V_0 (V)	*F*, Eq. [9] (V/cm)	*d* (nm)	*F*, Eq. [13] (V/cm)
2×10^{20}	1.9	3.3×10^6	10	7.9×10^6
			2	2.5×10^7
2×10^{20}	0.9	2.2×10^6	10	4.5×10^6
			2	1.3×10^7
5×10^{19}	0.9	1.1×10^6	10	3.3×10^6
			2	1.1×10^7

particles. This is due to the curvature of the metal surface. For large enough metal particles ($d > 100$ nm) the predictions of Eq. [13] tend asymptotically to those of Eq. [9], as expected. The fraction of the metal atoms at the metal–support–gas interface, which are affected by the electric field and are simultaneously exposed to the gas phase, is proportional to the metal dispersion, D. Because, however, the electric field increases with increasing dispersion, the total effect will be proportional to D^a, where $1 < a < 2$.

DISCUSSION

Two different model configurations of a catalytic system consisting of a noble metal supported on a TiO_2 carrier doped with higher valence cations have been studied in the framework of the metal–semiconductor contact theory. One configuration is described as metal overlayers of infinite dimension and the second one as spherical metal particles embedded within the semiconductor. In both cases, the driving force for charge transfer is the difference in the work function of the two materials or, alternatively, the difference in the electrochemical potentials. Because the work function of doped TiO_2 is lower than the work function of the metal, charge is transferred from the TiO_2 support to the metal and is located at the interface. Calculations performed for the aforementioned two configurations show that the maximum number of electrons transferred, compared to the number of metal atoms in the overlayer or the crystallite, is of the order of 0.1–0.4 *e*/atom for layers of one or two atoms thick or for crystallites with size in the range 1–2 nm. Such significant amounts of charge transferred can be considered to be partly due to the very high static dielectric constant of TiO_2 compared to other solid materials (titanates, such as $BaTiO_3$, also have very high dielectric constant). From this aspect, TiO_2 can be considered as a rather unique example of a support, favoring charge transfer to the supported metal.

Accurate estimation of the charge-transferred flux in the case of undoped TiO_2 is difficult because the donor concentration in the semiconductor is not known. The work function of stoichiometric, unreduced TiO_2 is 5.5 eV (44) (the Fermi level of stoichiometric TiO_2 will be near the middle of the band gap, $E_g(TiO_2) = 3.0$ eV, and $\Phi_{TiO_2} = \chi_{TiO_2} + E_g/2 = 4.0 + 1.5 = 5.5$ eV), which is similar to the metal work function. Therefore, no significant charge transfer is expected in this case. For reduced TiO_2, Ti^{3+} cations which are created, correspond to donor levels that decrease the work function. A work function of 4.1 eV has been reported by Sadeghi and Henrich (10), while a value of 4.6 eV has also been reported (44) for reduced TiO_2. What is not known, however, is the extent of reduction of TiO_2 in a supported catalyst, which defines the donor concentration and, moreover, whether the Ti^{3+} species are homogeneously distributed into the bulk or are located mainly in the surface region. Phenomenologically, though, reduced TiO_2 can be treated in the same manner as doped TiO_2 in the framework of the model of the present work.

The charge which is transferred is expected to lie at the metal–semiconductor interface, on the side of the metal. This can be explained by the following argument: A metal surface is an equipotential surface. Because the dielectric constant of TiO_2 is 130, the charge located at the interface will be 130 times larger than the charge at the free metal surface, even without taking into account the attractive contribution of the positively charged depletion region in the semiconductor. Therefore, the charge at the free metal surface is negligible.

It is still unclear in what way the electrons which are transferred to the metal–semiconductor interface can perturb the electronic structure of the metal crystallite, leading to modification of its chemisorptive and catalytic properties. Intuitively, one expects that whatever the interaction is, it will be more intense for small metal crystallites, for which the ratio e/M was found to be significant (Fig. 4) and the fraction of interface metal atoms is large. Although a detailed account of possible interaction routes is beyond the scope of this work, we can speculate on two different modes of electronic interaction, namely:

(a) long-range interactions, affecting the whole metal crystallite,

(b) short-range interactions, affecting the atoms at the gas–metal–support interface.

The former case implies modification of the electronic structure of the metal crystallite, such as the following:

(i) Changes in the *d*-band population. Chen *et al.* (21) have proposed that electronic modification might be due to rehybridization of electron orbitals in the presence of charge at the interface.

(ii) Shifting of the Fermi level and, as a consequence, of the work function. Theoretical calculations by Ward *et al.* (45) have shown that the Fermi level of Rh, Pd, and Pt is shifted when they are present as mono- or three-layer slabs on alumina surfaces. This shift is a consequence of charge transfer between the metal and the support. The charge transferred was found to be of the order of 0.1–0.2 *e*/atom.

(iii) Changes in the density of states at the Fermi level.

The short-range interaction can be considered as a consequence of the strong electric fields, which are present at the interface. The existence of strong electric fields (>0.1 V/nm) can have a significant impact on the adsorptive and catalytic properties of the metal atoms. The effect of an electric field on the adsorption of NO on Pt(111) and Rh(111) has been studied theoretically and experimentally (46–48). It was shown that for a field pointing away from the surface the binding energy of NO on Rh(111) is reduced by 15% (or about 4 kcal/mol) at a field of 3 V/nm. In stronger

fields, even the dissociation of NO on the surface can be induced. Theoretical calculations show that an electrostatic interaction can explain many aspects of the promoting or poisoning effect of several preadsorbed atoms on the metal surface (49). Vanselow and Mundschau (50) have observed the formation of high work function islands on a Pt surface on which TiO_2 has been deposited and has been heated above 800 K. They estimated that the induced electric field by the interaction of these islands with the rest of the surface is in the range 0.06–6 V/nm. It should be noted that the results obtained in the present study (Table 3) are in the same range.

The transfer of electrons from the support to the metal particles, or vice versa, also influences the electron structure of the support at the periphery of the metal particle. This part of the support can be either depleted or enriched in electrons. The affected region of the support, as deduced from the magnitude of the depletion length, W, can be quite large and might respond differently to various adsorbates. For example, in the depletion region of an n-type semiconductor the adsorption of electron donor adsorbates might be enhanced, while the adsorption of electron acceptor adsorbates might be hindered. This phenomenon can affect the catalytic behavior of the metal/semiconductor system via one of the following mechanisms:

- Creation of new catalytic sites on the support surface at the periphery of the metal particle.
- Enhancement of the spillover of intermediate species of the reaction from the support to the metal, or vice versa.

CONCLUSIONS

The following conclusions can be drawn from the results of the present study.

(a) The metal–semiconductor contact theory predicts that when a Group VIII metal is in contact with higher-valence doped or reduced TiO_2, a significant quantity of charge transfer can occur at the interface. The magnitude of charge transfer depends on the size of the metal particles and can be as high as 0.5 electrons per metal atom for crystallites smaller than 2 nm or less than 0.01 electrons per metal atom for crystallites larger than 10 nm.

(b) Titania is a rather unique example of a support favoring charge transfer, because it has a very high dielectric constant, as compared to other metal oxide semiconductors.

APPENDIX 1

1. Calculation of the Work Function of Doped TiO_2

The electronic energy levels for a semiconductor are shown schematically in Fig. 5. The upper edge of the valence band is of energy E_v, while the lower edge of the conduction band is of energy E_c. The Fermi level is located

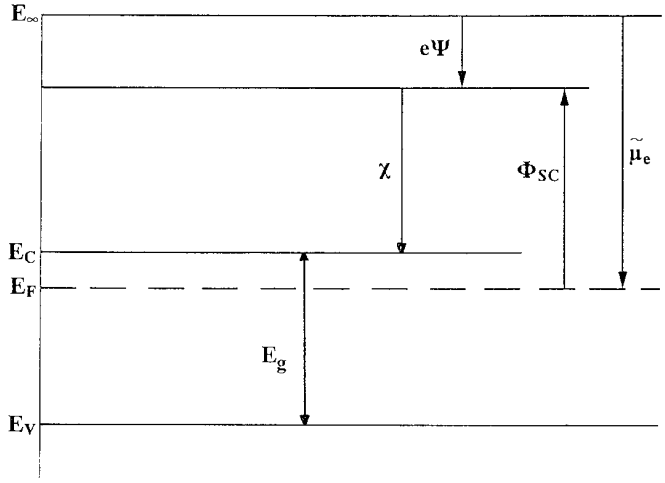

FIG. 5. The electronic energy level diagram for a semiconductor, with the component energy differences indicated. The diagram illustrates an n-type semiconductor.

inside the band gap and is closer to the conduction band for an n-type semiconductor or closer to the valence band for a p-type. The Fermi level is equivalent to the concept of the electrochemical potential of the semiconductor, $\tilde{\mu}_e$. The work function, Φ_{SC}, is defined from a thermodynamic point of view (51), as the difference between the Fermi level and the electrostatic potential right out of the semiconductor surface:

$$\Phi_{SC} = -\tilde{\mu}_e - e\Psi. \qquad [17]$$

The electron affinity, χ_{SC}, is defined as the difference between the edge of the conduction band and the electrostatic potential (40):

$$\chi_{SC} = -E_c - e\Psi. \qquad [18]$$

The position of the Fermi level can be manipulated by doping, which creates donor or acceptor levels in the band gap. For donor concentration, N_d, the electron concentration in the conduction band will be (41, 52)

$$n = N_d^+ + p, \qquad [19]$$

where N_d^+ is the concentration of the ionized donors, given by (53)

$$N_d^+ = N_d\left[1 - \frac{1}{1 + \frac{1}{2}\exp((E_d - E_F)/kT)}\right], \qquad [20]$$

with E_d being the donor energy level. The hole concentration, p, is generally written as

$$p = N_v\left[1 - \frac{1}{1 + \exp((E_v - E_F)/kT)}\right], \qquad [21]$$

while for the electron concentration, n;

$$n = N_c\frac{1}{1 + \exp((E_c - E_F)/kT)}. \qquad [22]$$

Combining Eqs. [20], [21], and [22], a relationship for the determination of E_F as a function of N_d, E_d, and T is obtained:

$$\frac{N_c}{1+\exp((E_c-E_F)/kT)} = N_d\left[1-\frac{1}{1+\frac{1}{2}\exp((E_d-E_F)/kT)}\right] + N_v\left[1-\frac{1}{1+\exp((E_v-E_F)/kT)}\right]. \quad [23]$$

Focusing on the semiconductor which is of interest in this study, i.e., TiO_2, doping with cations of valence higher than +4 (W^{6+}, for example), leads to the creation of a donor level near the conduction band. As a result, the Fermi level moves upward, close to the conduction band, and the work function decreases. This has been verified experimentally by electrical conductivity measurements (35).

2. Derivation of Eq. [6]

The charge density, ϱ, in the semiconductor depletion region is given by

$$\rho/e = [\text{ionized donors}] - \begin{bmatrix}\text{electron}\\ \text{density}\end{bmatrix} + \begin{bmatrix}\text{hole}\\ \text{density}\end{bmatrix} = N_d^+ - n + p. \quad [24]$$

The hole density, p, in the case of an n-type semiconductor (such as TiO_2) doped with a donor impurity is negligible and can be omitted from Eq. [24]. The concentration of ionized donors, N_d^+, can be derived from Eq. [20] after taking into account the effect of the potential V in the depletion region (39):

$$N_d^+ = N_d\left[1-\frac{1}{1+\frac{1}{2}\exp((-eV-E_d)/kT)}\right]. \quad [25]$$

The electron density, n, can be found similarly by suitable modification of Eq. [22],

$$n = n_\infty \exp\left(\frac{eV+E_F}{kT}\right), \quad [26]$$

with n_∞ given by Eq. [22]. The use of the exponential term $\exp((eV+E_F)/kT)$ instead of the exact term

$$1/1+\exp(-(eV+E_F)/kT)$$

is justified by the fact that the potential V is significant in a major part of the depletion region, so that the exponential term is much larger than unity. The error in using the approximate form becomes apparent only far away from the interface, where the number of transferred electrons is minimal anyway. Combining Eqs. [24], [25], and [26], Eq. [6] is obtained.

APPENDIX 2: LIST OF SYMBOLS

D	metal dispersion
d	metal crystallite diameter (nm)
E_c	lower edge of conduction band (eV)
E_d	donor level (eV)
E_F	Fermi energy (eV)
E_g	band gap (eV)
E_v	upper edge of valence band (eV)
e	electron charge (C)
F	electric field (V/cm)
N_c	density of states in the conduction band (cm^{-3})
N_d	donor concentration (cm^{-3})
N_d^+	ionized donor concentration (cm^{-3})
N_v	density of states in the valence band (cm^{-3})
n	electron concentration (cm^{-3})
n_e	number of transferred electrons
n_∞	electron concentration in semiconductor bulk (cm^{-3})
Q	electric charge per unit area (charge flux) (C/cm^2)
p	hole concentration (cm^{-3})
r	radial distance (cm)
r_M	metal crystallite radius (cm)
T	temperature (K)
V	potential (V)
V_0	contact potential (V)
W	depletion length (cm)

Greek

$\Delta\Psi_M^{SC}$	contact potential difference (V)
ε	relative dielectric constant
ε_o	vacuum permittivity (F/m)
ε_S	semiconductor permittivity (F/m)
$\tilde{\mu}_e$	electrochemical potential (eV)
$\tilde{\mu}_e^{eq}$	equilibrium electrochemical potential (eV)
ϱ, ϱ/e	charge density ($C\cdot cm^{-3}$, cm^{-3})
Φ	work function (eV)
Φ_{SB}	Schottky barrier (V)
χ_{SC}	semiconductor electron affinity (eV)
Ψ	electrostatic (outer) potential (V)

REFERENCES

1. Schwab, G. M., *in* "Advances in Catalysis" (D. D. Eley, H. Pines, and P. B. Weisz, Eds.), Vol. 27, p. 1. Academic Press, New York, 1978.
2. Solymosi, F., *Catal. Rev.* **1**, 233 (1967).
3. Baddour, R. F., and Deibert, M. C., *J. Phys. Chem.* **70**, 2173 (1966).
4. Kesraoui, S., Oukaci, R., and Blackmond, D. G., *J. Catal.* **105**, 432 (1987).
5. Angevaare, P. A. J. M., Hendrickx, H. A. C. M., and Ponec, V., *J. Catal.* **110**, 18 (1988).
6. Stevenson, S. A., Lisitsyn, A., and Knözinger, H., *J. Phys. Chem.* **94**, 1576 (1990).
7. Belton, D. N., Sun, Y.-M., and White, J. M., *J. Phys. Chem.* **88**, 5172 (1984).

8. Sexton , B. A., Hughes, A. E., and Foger, K., *J. Catal.* **77**, 85 (1982).
9. Kao, C.-C., Tsai, S.-C., and Chung, Y.-W., *J. Catal.* **73**, 136 (1982).
10. Sadeghi, H. R., and Henrich, V. E., *J. Catal.* **109**, 1 (1988).
11. Resasco, D. E., Weber, R. S., Sakellson, S., McMillan, M., and Haller, G. L., *J. Phys. Chem.* **92**, 189 (1988).
12. Yoshitake, H., and Iwasawa, Y., *J. Phys. Chem.* **96**, 1329 (1992).
13. Disdier, J., Herrmann, J.-M. and Pichat, P., *J. Chem. Soc. Faraday Trans. 1* **79**, 651 (1983).
14. Herrmann, J. M., *J. Catal.* **89**, 404 (1984).
15. Solymosi, F., Tombacz, I., and Kocsis, M., *J. Catal.* **75**, 78 (1982).
16. Mériaudeau, P., Ellestad, O. H., Dufaux, M., and Naccache, C., *J. Catal.* **75**, 243 (1982).
17. Raupp, G. B., and Dumesic, J. A., *J. Catal.* **97**, 85 (1986).
18. Herrmann, J. M., Gravelle-Rumeau-Maillot, M., and Gravelle, P. C., *J. Catal.* **104**, 136 (1987).
19. Aika, K., Ohya, A., Ozaki, A., Inoue, Y., and Yasumori, I., *J. Catal.* **92**, 305 (1985).
20. Ishihara, T., Harada, K., Eguchi, K., and Arai, H., *J. Catal.* **136**, 161 (1992).
21. Chen, H.-W., White, J. M., and Ekerdt, J. G., *J. Catal.* **99**, 293 (1986).
22. Yamamoto, N., Tonomura, S., and Tsubomura, H., *J. Electrochem. Soc.* **129**, 444 (1982).
23. Verwey, E. J. W., Haijman, P. W., Romeijn, F. C., and Oosterhoot, G. N., *Philips Res. Rep.* **5**, 173 (1950).
24. Akubuiro, E. C., and Verykios, X. E., *J. Catal.* **103**, 320 (1987).
25. Akubuiro, E. C., and Verykios, X. E., *J. Catal.* **113**, 196 (1988).
26. Akubuiro, E. C., Verykios, X. E., and Ioannides, T., *Appl. Catal.* **46**, 297 (1989).
27. Akubuiro, E. C., Ioannides, T., and Verykios, X. E., *J. Catal.* **116**, 590 (1989).
28. Ioannides, T., Verykios, X. E., Tsapatsis, M., and Economou, C., *J. Catal.* **145**, 491 (1994).
29. Zhang, Z., Kladi, A., and Verykios, X. E., *J. Catal.* **148**, 737 (1994).
30. Solymosi, F., Tombacz, I., and Koszta, J., *J. Catal.* **95**, 578 (1985).
31. Ioannides, T., and Verykios, X. E., *J. Catal.* **145**, 479 (1994).
32. Zhang, Z., Kladi, A., and Verykios, X. E., *J. Phys. Chem.* **98**, 6804 (1994).
33. Koussathana, M., Vamvouka, N., Tsapatsis, M., and Verykios, X. E., *Appl. Catal.* **80**, 99 (1992).
34. Koussathana, M., Vamvouka, N., and Verykios, X. E., *Appl. Catal.* **95**, 211 (1993).
35. Akubuiro, E. C., and Verykios, X. E., *J. Phys. Chem. Solids* **50**, 17 (1989).
36. Ponec, V., *in* "New Trends in CO Activation" (L. Guczi, Ed.), Vol. 64, p. 117, Studies in Surface Science and Catalysis. Elsevier, Amsterdam, 1991.
37. Tyagi, M. S., *in* "Metal-Semiconductor Schottky Barrier Junctions and Their Applications" (B. L. Sharma, Ed.). Plenum, New York, 1984.
38. Brillson, L. J., *Surf. Sci. Rep.* **2**, 123 (1982).
39. Henisch, H. K., *in* "Electrode Processes in Solid State Ionics" (M. Kleitz and J. Dupay, Eds.). Reidel, Dordrecht, Holland, 1976.
40. Sparnaay, M. J., *Surf. Sci. Rep.* **4**, 101 (1985).
41. Solymosi, F., *in* "Contact Catalysis" (Z. G. Szabó, D. Kalló, Eds.), Vol. 1, p 161. Elsevier, Amsterdam, 1976.
42. Jackson, J. D., "Classical Electrodynamics," 2nd ed. Wiley, New York, 1975.
43. Clark, R. J. H., *in* "Comprehensive Inorganic Chemistry" (J. C. Bailar, H. J. Emeléus, S. R. Nyholm, and A. F. Trotman-Dickenson, Eds.), 1st ed., Vol. 3, p. 376. Pergamon Press, New York, 1973.
44. Chung, Y. W., Lo, W. J., and Somorjai, G. A., *Surf. Sci.* **64**, 588 (1977).
45. Ward, T. R., Alemany, P., and Hoffmann, R., *in* "Environmental Catalysis" (J. N. Armor, Ed.), p. 140, ACS Symposium Series 552. Am. Chem. Soc., Washington, DC, 1994.
46. Kreuzer, H. J., and Wang, L. C., *J. Chem. Phys.* **93**, 6065 (1990).
47. Block, J. H., Kreuzer, H. J., and Wang, L. C., *Surf. Sci.* **246**, 125 (1991).
48. Madenach, R. P., Abend, G., Mousa, M. S., Kreuzer, H. J., and Block, J. H., *Surf. Sci.* **266**, 56 (1992).
49. Lang, N. D., Holloway, S., and Nørskov, J. K., *Surf. Sci.* **150**, 24 (1985).
50. Vanselow, R., and Mundschau, M., *J. Catal.* **103**, 426 (1987).
51. Reiss, H., *J. Phys. Chem.* **89**, 3783 (1985).
52. Sze, S. M., "Physics of Semiconductor Devices," 2nd ed. Wiley, New York, 1981.
53. Burns, G., "Solid State Physics." Academic Press, Orlando, 1985.